



**Search for pair production of the supersymmetric partner of the top quark in the  $\tilde{t}_1\tilde{t}_1 \rightarrow b\bar{b}e^\pm\mu^\pm\tilde{\nu}\tilde{\nu}$  decay channel at DØ**

The DØ Collaboration

URL <http://www-d0.fnal.gov>

(Dated: 1st April 2008)

A search for the lightest supersymmetric partner of the top quark,  $\tilde{t}_1$ , produced in  $p\bar{p}$  collisions at  $\sqrt{s}=1.96$  TeV has been performed using the DØ detector at the Fermilab Tevatron collider. Assuming the decay  $\tilde{t}_1 \rightarrow b\tilde{\nu}$  is dominant, leads to a final state with missing energy, an electron and a muon. A good agreement with Standard Model expectation has been observed in a dataset corresponding to an integrated luminosity of  $1.1 \text{ fb}^{-1}$ . New limits at 95% confidence level in the plane  $(m_{\tilde{t}_1}, m_{\tilde{\nu}})$  have been set.

*Preliminary Results for Winter 2008 Conferences*

## I. INTRODUCTION

Supersymmetry (SUSY) [1] is one of the most promising ways to solve crucial problems of the Standard Model (SM). This spacetime symmetry links bosons to fermions by introducing supersymmetric partners (sparticles) to all SM particles. Hence the quark helicity states  $q_R$  and  $q_L$  have scalar partners  $\tilde{q}_R$  and  $\tilde{q}_L$ . But whereas  $\tilde{q}_R$  and  $\tilde{q}_L$  are supposed to be mass eigenstates for the two first generations, a strong mixing may appear for the third one, leading to a significant splitting between the mass eigenstates. The result is that the lightest SUSY partner of the top quark, stop  $\tilde{t}_1$ , may be light enough to be produced at the Tevatron.

In a  $p\bar{p}$  collider, scalar top pairs are expected to be produced via  $q\bar{q}$  annihilation and  $gg$  fusion. If R-parity is conserved and if the  $\tilde{t}_1$  is lighter than the top quark,  $\tilde{t}_1$  may decay into  $b\tilde{\chi}_1^+$ ,  $c\tilde{\chi}_1^0$ ,  $bl\tilde{\nu}$  or  $b\bar{l}\tilde{\nu}$ . The  $b\tilde{\chi}_1^+$  and  $b\bar{l}\tilde{\nu}$  channels tend to be disfavored by LEP searches [2]. A search for the decay  $\tilde{t}_1 \rightarrow c\tilde{\chi}_1^0$  has been previously reported by DØ [3]. In this paper we present the search for the scalar top quark decaying to  $bl\tilde{\nu}$ .

In our search, we assume that the sneutrino is the Lightest Supersymmetric Particle (LSP). In that case, production of scalar top pairs will result in a final state with two opposite-sign leptons, two b-jets and missing energy that comes mainly from undetected sneutrinos. In this study we explore the  $e\mu$  final state:  $b\bar{b}e\mu\tilde{\nu}\tilde{\nu}$ . A similar search using one third of this data set was reported previously [4].

## II. DØ DETECTOR

The DØ detector [5] comprises a central tracking system surrounded by a liquid-argon sampling calorimeter and a system of muon detectors. Charged particles are reconstructed using a system of multi-layer silicon detector and eight double layers of scintillating fibers in a 2T magnetic field produced by a superconducting solenoid. After passing through the calorimeter, muons are detected in the muon detector comprising three layers of tracking detectors and scintillation counters. Events containing electrons or muons are selected for offline analysis by an online trigger system. A set of dilepton triggers has been used to tag the presence of electrons and muons based on their energy deposit in the calorimeter, hits in the muon detectors and tracks in the tracking system.

## III. DATA AND MONTE CARLO SAMPLES

The data used in this analysis were collected from April 2002 to February 2006. Low  $p_T$   $e\mu$  triggers were chosen so as to be sensitive to low mass differences between the stop and the sneutrino. The total integrated luminosity is  $(1100 \pm 71)$   $\text{pb}^{-1}$ . Trigger efficiencies were estimated from data.

For the simulation of the three-body decays of the  $\tilde{t}_1$ , the Monte Carlo generators Comphep [6] and Pythia 6.4 [7] were used for the generation of the particles and the hadronization of the quarks. We assumed that the decay  $\tilde{t}_1 \rightarrow bl\tilde{\nu}$  occurs through a virtual chargino  $\tilde{\chi}_1^\pm$  with a branching ratio of 100% and that the width of the sneutrino is close to zero. We considered a range of stop mass points from 100 to 200  $\text{GeV}/c^2$  in steps of 10  $\text{GeV}/c^2$ . The sneutrino masses extend from 40 to 140  $\text{GeV}/c^2$  in steps of 10 to 20  $\text{GeV}/c^2$ . For each mass point, 10,000 events were generated. The nominal theoretical cross section for the production of scalar top pairs, shown on Fig. 1, was obtained from Prospino2 [8] with CTEQ6.1M PDF's and for a renormalization scale and a factorization scale,  $\mu_{rf}$ , equal to the stop mass. The uncertainty associated with the PDF's, estimated following [9], was combined quadratically with the variation obtained when  $\mu_{rf}$  was modified by a factor of 2 or 0.5. The relative uncertainties range from 17 to 20%.

Background events arise from two independent sources. Physics background comes from SM processes with isolated electron and muon pairs, namely:  $Z/\gamma^* \rightarrow \tau^+\tau^-$ , WW, WZ, ZZ and  $t\bar{t}$ . This background was simulated with Pythia. Channels involving the Z boson have been reweighted as a function of the  $p_T$  of the Z to reproduce the experimental differential cross section  $d\sigma(Z)/dp_T$ . The second background source is due to either mis-identified electrons, muons or jets, mismeasured  $\cancel{E}_T$ , or electrons or muons from multijet processes which pass lepton isolation requirements that are presented below. These backgrounds, which are labeled as instrumental in this paper, are estimated from data.

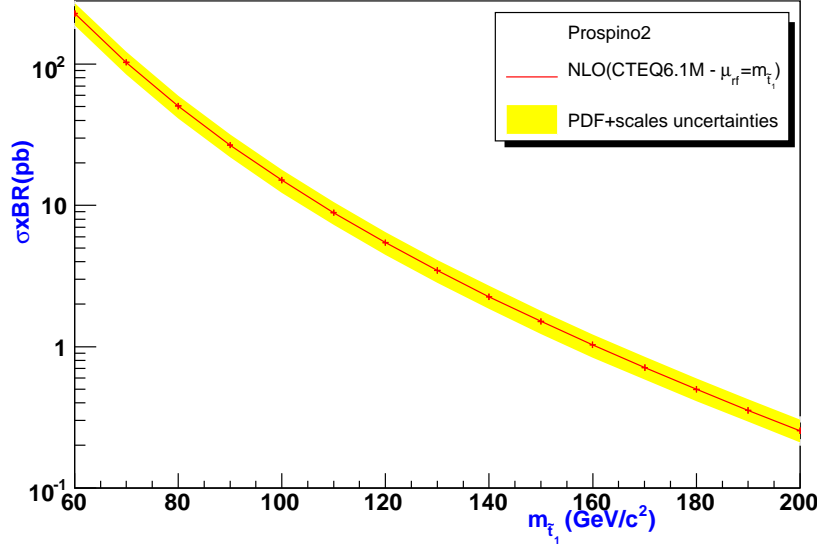


Figure 1: PROSPINO NLO Cross section as a function of the stop mass. The yellow band denotes the uncertainty on the theoretical predictions (PDF and renormalization and factorization scales)

The  $Z/\gamma^* \rightarrow \tau^+\tau^-$  cross section is estimated with CTEQ6.1M PDFs as  $\sigma(Z/\gamma^* \rightarrow \tau^+\tau^-) = \sigma_{LO} \times K_{QCD}(Q^2)$  with the LO cross section calculated by Pythia with LO PDF and the  $K_{QCD}$  at NNLO with NLO PDF, according to [10, 11]. WW, ZZ and WZ cross sections are calculated in [11] with MCMF using CTEQ6.1M PDFs. The  $t\bar{t}$  cross section is calculated at NNLO [12]. Errors due to the PDF uncertainty and to the variation of factorization and renormalization scales are estimated in [10, 11].

#### IV. EVENT SELECTION

In each event we require a reconstructed primary vertex with  $|z_{vtx}| < 60$  cm, at least one muon with  $p_T > 8$  GeV/c and one electron with  $p_T > 15$  GeV/c.

##### A. Muon and Electron identification

A muon candidate in the region  $|\eta| < 2$  is selected using the following criteria:

- wire and scintillator hits in the inner and the outermost layers of the muon detector, matched to the central tracking detector,
- timing cuts to reject cosmic muons,
- at least one hit in the silicon tracker,
- isolation from calorimeter energy:  $E(0.4) - E(0.1) < 2.5$  GeV, where  $E(R)$  is the transverse energy measured in the calorimeter in a radius  $R = \sqrt{(\Delta\eta)^2 + (\Delta\phi)^2}$  around the muon,
- isolation from other tracks:  $\sum_i^{R=0.5} p_T(i) < 2.5$  GeV/c, where the sum runs over all charged tracks in a cone of radius  $R = 0.5$  around the muon.

An electron candidate satisfies the following criteria:

- the ratio of the electromagnetic (EM) energy to the total shower energy should be greater than 0.9,
- isolation from the other energy deposit in the calorimeter  $[E(0.4) - E_{EM}(0.2)]/E_{EM}(0.2) < 0.15$  where  $E(R)$  and  $E_{EM}(R)$  are the total and EM energy, deposited in a cone of radius  $R$  centered around the electron candidate,
- the lateral and the longitudinal shapes of the EM energy should be consistent with those of an electron.

A likelihood discriminant combining the energy deposited in the calorimeter and the associated track is used to reduce contamination from photons and jets faking electrons. Good electrons have a likelihood value greater than 0.85 and a track  $p_T$  greater than 8 GeV/c. Only central electrons ( $|\eta_{det}| < 1.1$ ) are considered.

Jets are reconstructed from the energy deposition in the calorimeter towers using the RunII cone algorithm [13] with radius  $R_{cone} = 0.5$ . Only jets with  $p_T > 15$  GeV/c and  $|\eta| < 2.5$  are considered. The  $\cancel{E}_T$  is calculated using all calorimeter cells, corrected for the energy calibration of the reconstructed jets, for the momentum of reconstructed muons and for the electromagnetic scale for identified electromagnetic objects.

Events with electron candidates sharing the same track with any good muon candidate were rejected. The electron and muon in an event are required to be isolated from each other ( $\Delta R(e, \mu) > 0.5$ ) and from a jet ( $\Delta R((e, \mu), jet) > 0.5$ ).

## B. Selection cuts

The selection cuts that have been applied to the analysis are listed in Table I, along with the number of events surviving at each step for the data, for each background component, and for two signal samples ( $m_{\tilde{\tau}_1} = 140$  GeV/c<sup>2</sup> and  $m_{\tilde{\nu}} = 110$  GeV/c<sup>2</sup>;  $m_{\tilde{\tau}_1} = 170$  GeV/c<sup>2</sup> and  $m_{\tilde{\nu}} = 90$  GeV/c<sup>2</sup>). The instrumental background is estimated from data at the Cut0 level. An exponential fit is performed to the  $\cancel{E}_T$  distribution in the range 0-35 GeV, after subtraction of the Standard Model contribution.

Table I: Number of data and MC events selected at the various stages of the analysis. The quoted uncertainties are statistical only.

	Cut0	Cut1	Cut2	Cut3
	1 electron	$\cancel{E}_T \gtrsim 30$ GeV	$\Delta\phi(e, \cancel{E}_T) \gtrsim 0.4$ rad	$M_T(\mu, \cancel{E}_T) \gtrsim 20$ GeV/c <sup>2</sup>
	1 muon	$\text{Sig}(\cancel{E}_T) \gtrsim 4$	$\Delta\phi(\mu, \cancel{E}_T) \gtrsim 0.4$ rad	$M_T(e, \cancel{E}_T) \gtrsim 20$ GeV/c <sup>2</sup>
				$\Delta\phi(e, \cancel{E}_T) + \Delta\phi(\mu, \cancel{E}_T) \gtrsim 2.9$ rad
Instr. bkg	188 ± 14	21 ± 5	15 ± 4	13 ± 3
$Z/\gamma^* \rightarrow \tau^+\tau^-$	458 ± 5	23 ± 1	5.9 ± 0.6	0.7 ± 0.2
WW	51.8 ± 0.7	33.2 ± 0.5	31.4 ± 0.5	30.2 ± 0.5
WZ	7.1 ± 0.3	4.8 ± 0.2	4.2 ± 0.2	3.8 ± 0.2
ZZ	1.7 ± 0.1	0.7 ± 0.1	0.6 ± 0.1	0.5 ± 0.1
tt	29.7 ± 0.6	23.5 ± 0.5	20.0 ± 0.5	16.4 ± 0.4
total bkg	737 ± 15	107 ± 5	77 ± 4	64 ± 4
data	735	106	71	61
$m_{\tilde{\tau}_1} = 140$ GeV/c <sup>2</sup>	34 ± 1	10.6 ± 0.7	8.4 ± 0.7	6.0 ± 0.6
$m_{\tilde{\nu}} = 110$ GeV/c <sup>2</sup>				
$m_{\tilde{\tau}_1} = 170$ GeV/c <sup>2</sup>	26.3 ± 0.7	19.4 ± 0.6	17.6 ± 0.6	16.1 ± 0.5
$m_{\tilde{\nu}} = 90$ GeV/c <sup>2</sup>				

Cut0 corresponds to the requirement of one electron and one muon (with the above selection criteria) in the event. To remove a large part of the instrumental background as well as events coming from  $Z/\gamma^* \rightarrow \tau^+\tau^-$ , the missing transverse energy  $\cancel{E}_T$  is required to be greater than 30 GeV (Cut1 - Fig. 2). A minimum  $\cancel{E}_T$  significance of 4 is required (Fig. 5 in the appendix), where the  $\cancel{E}_T$  significance is defined by normalizing  $\cancel{E}_T$  to a measure of the jet energy resolution projected onto the  $\cancel{E}_T$  direction. The  $Z/\gamma^* \rightarrow \tau^+\tau^-$  background is further reduced by selections on the

azimuthal angles between the leptons and  $\vec{E}_T$ ,  $\Delta\phi(e, \vec{E}_T)$  and  $\Delta\phi(\mu, \vec{E}_T)$  (Cut2 - Fig. 3). Leptons from  $Z/\gamma^* \rightarrow \tau^+\tau^-$  events and poorly reconstructed leptons from the instrumental background events are correlated with  $\vec{E}_T$ . This gives rise to higher event populations at high and low values of the azimuthal angle difference between the leptons and  $\vec{E}_T$  with a low value of the angular difference for one lepton being correlated with a high value for the others. The transverse mass between the leptons and  $\vec{E}_T$ , defined by  $M_T(l, \vec{E}_T) = \sqrt{(E_T^l + \vec{E}_T)^2 - (p_X^l + \vec{E}_X)^2 - (p_Y^l + \vec{E}_Y)^2}$ , has low values for these events (Fig. 6 in the appendix). To remove this background a selection is applied on the transverse masses as well as on the sum of the  $\phi$  differences between the leptons and  $\vec{E}_T$  (Cut3 - Fig. 7 in the appendix).

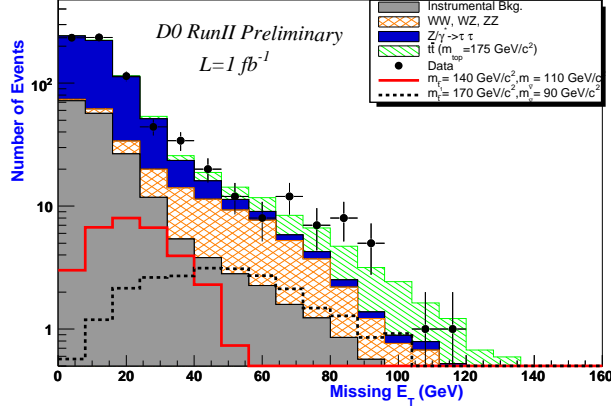


Figure 2: The missing transverse energy distribution after Cut0 for data (dots), simulated (filled areas) background and signal expectations for  $m_{\tilde{\tau}_1} = 140 \text{ GeV}/c^2$  and  $m_{\tilde{\nu}} = 110 \text{ GeV}/c^2$  (solid line) or  $m_{\tilde{\tau}_1} = 170 \text{ GeV}/c^2$  and  $m_{\tilde{\nu}} = 90 \text{ GeV}/c^2$  (dashed line).

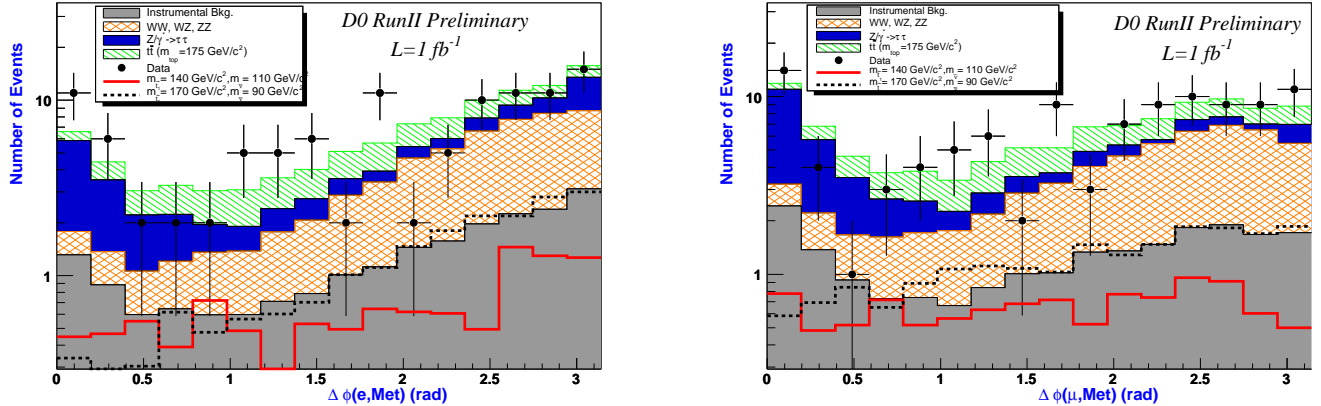


Figure 3: The  $\Delta\phi(e, \vec{E}_T)$  and  $\Delta\phi(\mu, \vec{E}_T)$  distributions for data (dots), simulated (filled areas) background and signal expectations for  $m_{\tilde{\tau}_1} = 140 \text{ GeV}/c^2$  and  $m_{\tilde{\nu}} = 110 \text{ GeV}/c^2$  (solid line) or  $m_{\tilde{\tau}_1} = 170 \text{ GeV}/c^2$  and  $m_{\tilde{\nu}} = 90 \text{ GeV}/c^2$  (dashed line), after Cut1.

## V. RESULTS

Signal efficiencies reach a value of 9% for large mass differences but decrease to negligible values for  $\Delta m = m_{\tilde{\tau}_1} - m_{\tilde{\nu}} = 20 \text{ GeV}/c^2$  (see Fig. 8 in the appendix).

The expected number of background and signal events depend on several measurements and parametrizations which each introduce a systematic uncertainty: luminosity (6.1%), electron identification efficiency (5.5%), muon identification and isolation efficiencies (0.7-2%), jet energy scale (12-16%), instrumental background (5%), and PDFs (6%). These systematic errors (except the luminosity and the instrumental background) are obtained by varying sequentially each affected quantity within  $\pm 1\sigma$ , where  $\sigma$  accounts for the relative efficiency resolution between data and simulation before any selection. The instrumental background systematic uncertainty is estimated by varying the exponential fit parameters within  $\pm 1\sigma$  of their errors.

A good agreement between data and SM expectation has been observed. Therefore upper limits at 95% C.L. on the production cross section of stop pairs may be evaluated. For this we have used the frequentist approach implemented in the TLimit program [14]. To increase our sensitivity to the stop signal, two topological variables were used:  $S_T$ , defined as the scalar sum of the muon  $p_T$ , the electron  $p_T$  and the missing transverse energy, and  $H_T$  which is equal to the  $p_T$  sum of the jets. The distributions of these variables after Cut3 are given on Fig. 9 in the appendix. WW and instrumental background populate low values of  $S_T$  and  $H_T$  while top pairs have large values for both variables. The signal distribution depends on the mass values with low values of  $\Delta m = m_{\tilde{t}_1} - m_{\tilde{\nu}}$  having low values of  $S_T$  and  $H_T$ . Hence the systematic uncertainty coming from the instrumental backgrounds affect low  $\Delta m = m_{\tilde{t}_1} - m_{\tilde{\nu}}$  signal points. The limit calculation was performed for each set of masses. The following bins have been used to compute the limits:  $S_T$ : 0–70, 70–120, > 120 and  $H_T$ : 0–15, 15–60, 60–120, > 120. The first bin in  $H_T$  corresponds to events without jets. The number of events for each ( $S_T, H_T$ ) bin are given in Tables II and III.

Table II: Number of data and MC events for  $S_T$  and  $H_T$  bins. The quoted uncertainties are statistical only.

$H_T$	$S_T$					
	0-70		70-120		>120	
	Data	MC	Data	MC	Data	MC
0-15	1	0.3± 0.3	15	13± 2	12	19± 2
15-60	1	0± 0	6	4.2± 0.9	11	8± 1
60-120	0	0± 0	1	1.6± 0.6	8	9± 1
>120	0	0.0± 0.0	0	0.9± 0.4	6	7± 1

Table III: Number of signal events ( $m_{\tilde{t}_1} = 170 \text{ GeV}/c^2$ ,  $m_{\tilde{\nu}} = 90 \text{ GeV}/c^2$ ) for  $S_T$  and  $H_T$  bins. The quoted uncertainties are statistical only.

$H_T$	$S_T$					
	0-70		70-120		>120	
	S	S/B	S	S/B	S	S/B
0-15	0.02± 0.02	0.07	0.28± 0.07	0.02	2.5± 0.2	0.13
15-60	0.01± 0.01	0.025	1.5± 0.2	0.32	5.9± 0.3	1.29
60-120	0.01± 0.01	-	1.1± 0.1	0.68	3.4± 0.3	0.39
>120	-	-	0.38± 0.08	0.30	1.1± 0.1	0.14

The exclusion domain is shown in Fig. 4 in the plane ( $m_{\tilde{t}_1}, m_{\tilde{\nu}}$ ). The effect of the cross section uncertainties (PDF's and renormalization and factorization scales) is represented by a band around the observed limit. For large mass differences, a stop mass lower than 175  $\text{GeV}/c^2$  is excluded. A sensitivity up to  $\Delta m = m_{\tilde{t}_1} - m_{\tilde{\nu}} = 30$  (40)  $\text{GeV}/c^2$  is observed for stop masses of 100 (140)  $\text{GeV}/c^2$ . The expected sensitivity has increased for larger  $\Delta m$  regions by about 15  $\text{GeV}/c^2$  with respect to the results of the combined ( $e\mu, \mu\mu$ ) analysis [4]. A good agreement between the expected and observed limits has now been obtained.

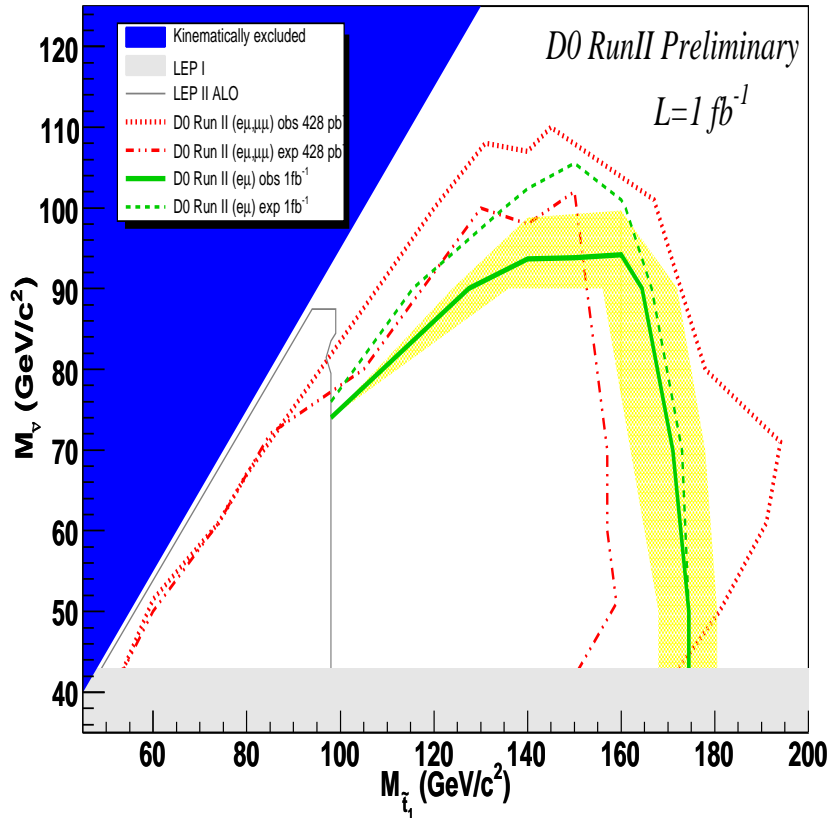


Figure 4: The 95% C.L. exclusion in the stop mass versus sneutrino mass plane. Dark blue and light grey areas represent the kinematically forbidden region and the LEP I exclusion respectively. The dark grey full line is the LEP II exclusion. The red dashed and dotted line and the red dotted line denote the expected and observed limit respectively [4] with  $428 \text{ pb}^{-1}$  ( $(e, \mu)$  and  $(\mu, \mu)$  channels combined). The thick and the dashed green lines represent the exclusion limits with  $1.1 \text{ fb}^{-1}$  for the  $(e, \mu)$  channel. The dashed line is the expected limit and the full line is the observed limit. The yellow band around the observed limit denotes the effect of the stop cross section uncertainties.

## VI. CONCLUSION

A search for stop pair production in  $p\bar{p}$  collisions at 1.96 TeV has been performed in a data sample of  $1.1 \text{ fb}^{-1}$ . The final state considered was one electron, one muon and large missing transverse energy. No deviation from the Standard Model expectation has been observed. Exclusion domains in the plane  $(m_{\tilde{t}_1}, m_{\tilde{\nu}})$  have been obtained. For larger mass differences between the stop and the sneutrino, the expected sensitivity has increased by about  $15 \text{ GeV}/c^2$  with respect to the results of the combined  $(e\mu, \mu\mu)$  analysis [4]. A good agreement between the expected and observed limits has now been achieved.

## Acknowledgments

We thank the staffs at Fermilab and collaborating institutions, and acknowledge support from the DOE and NSF (USA); CEA and CNRS/IN2P3 (France); FASI, Rosatom and RFBR (Russia); CAPES, CNPq, FAPERJ, FAPESP and FUNDUNESP (Brazil); DAE and DST (India); Colciencias (Colombia); CONACyT (Mexico); KRF (Korea); CONICET and UBACyT (Argentina); FOM (The Netherlands); PPARC (United Kingdom); MSMT (Czech Republic); CPC Program, CFI, NSERC and WestGrid Project (Canada); BMBF and DFG (Germany); SFI (Ireland); Research

Corporation, Alexander von Humboldt Foundation, and the Marie Curie Program.

---

- [1] P. Fayet and S. Ferrara, *Supersymmetry*, Phys. Rep. **32**, 249 (1977).  
H.P. Nilles, *Supersymmetry, supergravity and particle physics*, Phys. Rep. **110**, 1 (1984).
- [2] [http://lepsusy.web.cern.ch/lepsusy/www/squarks-summer04/stop\\_combi\\_208\\_final.html](http://lepsusy.web.cern.ch/lepsusy/www/squarks-summer04/stop_combi_208_final.html).
- [3] DØ Collaboration, “Search for Scalar Top Quarks in Acoplanar Charm Jet + Missing Energy Events” , 5436-CONF (2007).
- [4] V.M. Abazov *et al.* (DØ Collaboration), Phys. Lett. B **659**, 500 (2008).
- [5] V.M. Abazov *et al.* (DØ Collaboration), The upgraded DØ detector, Nucl. Instrum.Methods Phys. Res. **A 565**, 463 (2006).
- [6] A. Pukhov *et al.* CompHEP - User’s manual for version 3.3 arXiv:hep-ph/9908288.  
A.S. Belyaev *et al.* CompHEP - PYTHIA interface arXiv:hep-ph/0101232.
- [7] T. Sjöstrand, S. Mrenna and P. Skands, JHEP **05**, 026 (2006).
- [8] W. Beenaker, R. Hoepker, M. Spira hep-ph/9611232 - <http://www.ph.ed.ac.uk/~tplehn/prospino>.
- [9] J. Pumplin *et al.* JHEP **207**,012 (2002) 012 D. Stump *et al.* JHEP **310**, 046 (2003).
- [10] C.R. Hamberg, W.L. van Neerven and T. Matsuura, Nucl. Phys. **B359**, 343 (1991) , Erratum-ibid. **B644**, 403 (2002).
- [11] T. Nunnemann, “Drell-Yan, Z, W cross-sections“ [http://www-clued0.fnal.gov/~nunne/cross-sections/nnlo\\_xsect.html](http://www-clued0.fnal.gov/~nunne/cross-sections/nnlo_xsect.html).
- [12] N. Kidonakis, R. Vogt, Int. J. Mod. Phys **A20**, 3171 (2005).
- [13] G.C Blazey *et al.*, in *Proceedings of the Workshop: QCD and Weak Boson Physics in Run II*, edited by U.Baur, R.K. Ellis, and D. Zeppenfeld, Fermilab-Pub-00/297 (2000).
- [14] <http://root.cern.ch/root/html/TLimit.html> and references therein.

## Appendix

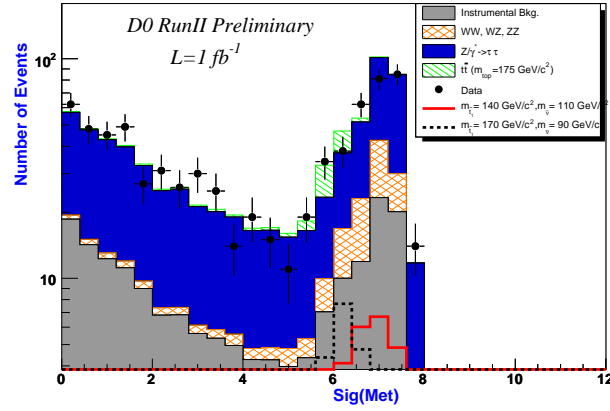


Figure 5: The significance  $\mathcal{E}_T$  distribution for data (dots), simulated (filled areas) background and signal expectations for  $m_{\tilde{\tau}_1} = 140 \text{ GeV}/c^2$  and  $m_{\tilde{\nu}} = 110 \text{ GeV}/c^2$  (solid line) or  $m_{\tilde{\tau}_1} = 170 \text{ GeV}/c^2$  and  $m_{\tilde{\nu}} = 90 \text{ GeV}/c^2$  (dashed line), after Cut0.

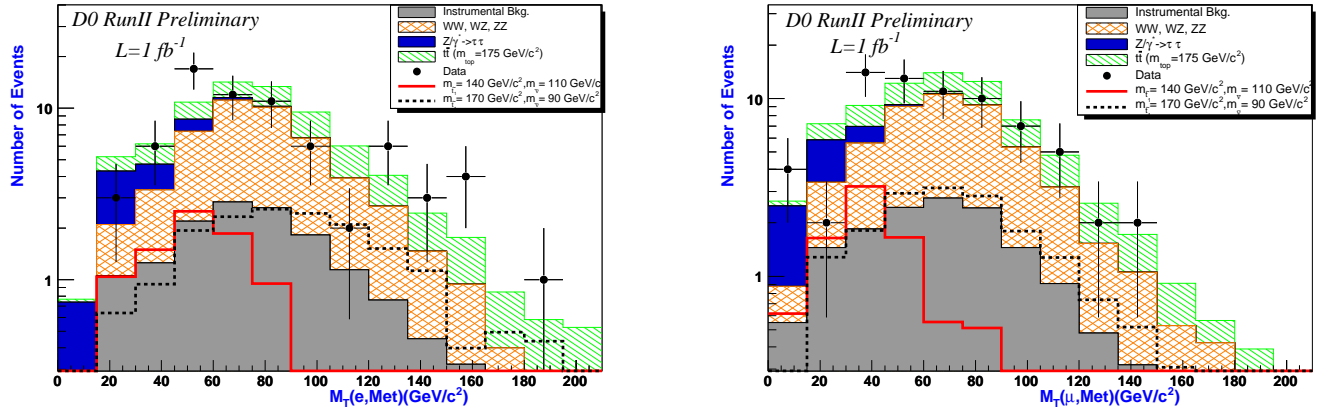


Figure 6: The transverse masses  $M_T(e, \text{Met})$  (left) and  $M_T(\mu, \text{Met})$  (right) distributions for data (dots), simulated (filled areas) background and signal expectations for  $m_{\tilde{\tau}_1} = 140 \text{ GeV}/c^2$  and  $m_{\tilde{\nu}} = 110 \text{ GeV}/c^2$  (solid line) or  $m_{\tilde{\tau}_1} = 170 \text{ GeV}/c^2$  and  $m_{\tilde{\nu}} = 90 \text{ GeV}/c^2$  (dashed line), after Cut2.

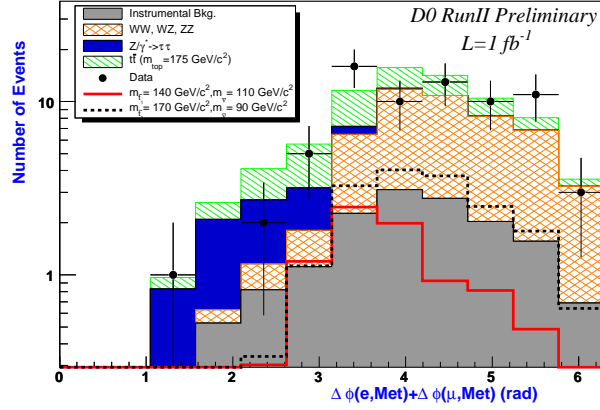


Figure 7: The  $\Delta\phi(e, \cancel{E}_T) + \Delta\phi(\mu, \cancel{E}_T)$  distribution for data (dots), simulated (filled areas) background and signal expectations for  $m_{\tilde{t}_1} = 140 \text{ GeV}/c^2$  and  $m_{\tilde{\nu}} = 110 \text{ GeV}/c^2$  (solid line) or  $m_{\tilde{t}_1} = 170 \text{ GeV}/c^2$  and  $m_{\tilde{\nu}} = 90 \text{ GeV}/c^2$  (dashed line), after Cut2.

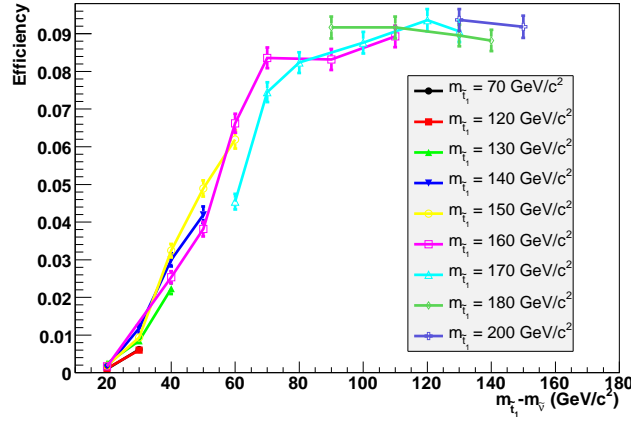


Figure 8: Selection efficiency for stop masses from 70-220  $\text{GeV}/c^2$  after Cut3 as a function of the mass difference between the stop mass and the sneutrino mass  $\Delta m = m_{\tilde{t}_1} - m_{\tilde{\nu}}$ .

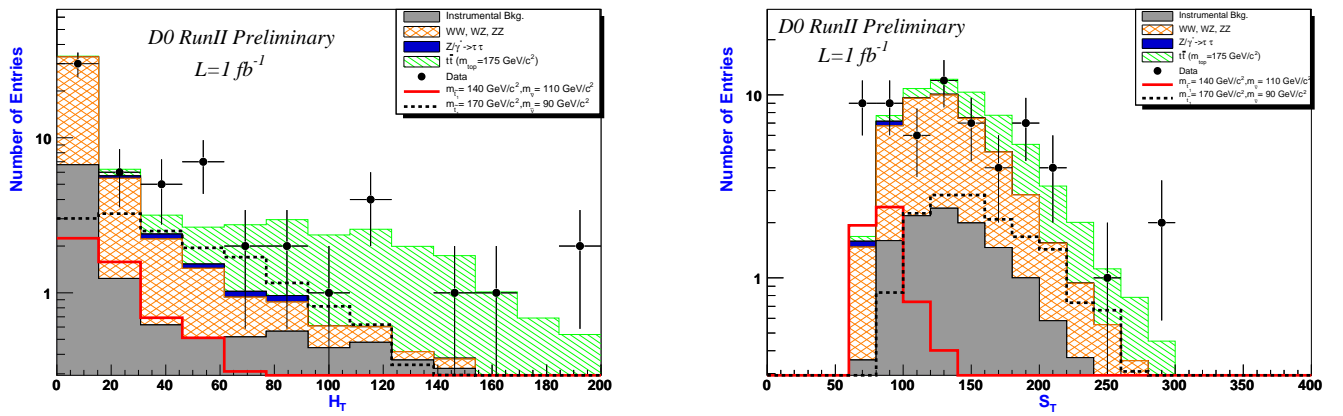


Figure 9: The  $H_T$  (left) and  $S_T$  (right) distributions for data (dots), simulated (filled areas) background and signal expectations for  $m_{\tilde{t}_1} = 140 \text{ GeV}/c^2$  and  $m_{\tilde{\nu}} = 110 \text{ GeV}/c^2$  (solid line) or  $m_{\tilde{t}_1} = 170 \text{ GeV}/c^2$  and  $m_{\tilde{\nu}} = 90 \text{ GeV}/c^2$  (dashed line), after Cut3.